Supplement of Earth Syst. Dynam., 16, 1237–1266, 2025
https://doi.org/10.5194/esd-16-1237-2025-supplement


Earth System Dynamics
Open Access
EGU

*Supplement of*

# Diagnosing aerosol–meteorological interactions on snow within Earth system models: a proof-of-concept study over High Mountain Asia

**Chayan Roychoudhury et al.**

*Correspondence to:* Chayan Roychoudhury (croychoudhury@arizona.edu)

## S1. XGBoost Model Implementation and Hyperparameter Optimization

We used the XGBoost model using the Scikit-Learn wrapper interface (within the `xgboost` package) to predict snow cover fraction (SCF) across different regions of High Mountain Asia (HMA). Our implementation followed a rigorous hyperparameter optimization approach using adaptive Tree-Parzen estimator algorithm (ATPE) via the `hyperopt` library in Python. Below, we provide the complete methodology to ensure reproducibility of our model.

### S1.1 Model Pre-processing

Models were trained separately for each combination of:

- Data source (ERA5/CAMS-EAC4, MERRA-2, MATCHA)
- Region (6 HMA subregions)
- Month (May, June, July)
- Construct type (original target (SCF) from MODIS, model target (SCF) from each reanalysis)

Our dataset had 22 predictors (six aerosol, 15 meteorological and one elevation) which we used for fitting the XGBoost model to SCF (from MODIS and the models/reanalysis).

### S1.1. Model Configuration

All models were implemented with the following specifications:

**Table S1.** XGBoost model specifications.

| Parameter | Configuration |
|---|---|
| Objective Function | Mean Squared Error |
| Random Seed | 24 |
| Hardware | GPU (NVIDIA A100) |
| Tree Method | gpu_hist |
| n_jobs | 1 |

We used a different cross-validation approach in our model, where we initialized the XGBoost model with a set of hyperparameters, split our dataset into 5 folds (that gives a training and a validation subset), and fit the XGBoost model to each training subset. We then finally fit the entire dataset with the XGBoost model and optimized it with `hyperopt`.

### S1.2 Hyperparameter Optimization

We used the adaptive Tree-structured Parzen Estimator algorithm within the *hyperopt* framework to efficiently search the following hyperparameter space for each model:

**Table S2.** Hyperparameter specifications.

| Hyperparameter | Range | Sampling Distribution |
|---|---|---|
| Maximum tree depth | 6-10 | Uniform (integer values) |
| Minimum child weight | 10-100 | Uniform (steps of 10) |
| Number of estimators | 500-1100 | Uniform |
| Learning rate | 0.01-1.0 | Log-uniform |
| Gamma | 0-5 | Uniform (steps of 0.2) |
| L2 regularization (reg_lambda) | 0-100 | Uniform |
| Subsample ratio | 0.8-1.0 | Uniform |
| Hyperopt objective to minimize | Model MAE (mean absolute error) | |

For each regional model, we conducted approximately 140 trial iterations (20 × number of hyperparameters = 7) with an early stopping criterion that terminated the search after 15% of trials showed no improvement in performance.

Each model's final performance was evaluated using multiple metrics:

- Mean Absolute Error (MAE)
- Root Mean Squared Error (RMSE)
- Coefficient of determination ($R^2$)
- Pearson's correlation coefficient ($\rho$)

**S1.4 SHAP Value Calculation**

To quantify the contribution of individual predictors and their interactions to model predictions, we utilized the SHapley Additive exPlanations (SHAP) values calculated through XGBoost's native implementation. Rather than using the separate `shap` library, we employed XGBoost's built-in functionality via the *pred_contribs=True* and *pred_interactions=True* parameters in the booster's predict method to also account for interactions. This approach allows us to leverage GPU acceleration through the *gpu_predictor* parameter, significantly reducing computation time for our high-dimensional dataset. An important thing to note is that SHAP values were calculated for both individual feature contributions and pairwise interactions, accounting for complex interdependencies between variables. The XGBoost native implementation is similar to the standard SHAP algorithm, producing contribution values that sum to the difference between each prediction and the expected value of the model output.

We modified the SHAP values to a normalized contribution (defined as SHAPc) by averaging the absolute SHAP values and dividing by their sum. The steps are as follows,

1. Extracted the interaction matrices from the SHAP values, excluding the bias term (expected/base value).
2. Computed the absolute values to focus on magnitude of influence instead of direction.
3. Normalized these values by dividing by the sum of all absolute interaction effects for each sample, then multiplied by 100 to express the SHAP contributions as percentages.
4. Applied statistical functions (mean, standard deviation, and various percentiles: 5%, 25%, 50%, 75% and 95%) across samples to characterize the distribution of interaction effects.
5. Maintained the symmetry of interaction effects by doubling off-diagonal values in the interaction matrix, since interactions between features A and B are commutative.
6. Processed the interaction matrices to create tables that distinguish between main effects (single predictors) and interaction effects (predictor pairs). We then preserved regional and temporal context by tagging each interaction with its corresponding month, region, and data source.

**S1.5 Computational Environment**

All models were developed using Python 3.8 with the following key libraries:

- `xgboost 1.7.4`
- `hyperopt 0.2.7`
- `scikit-learn 1.4.2`

**Supplementary Figures.**

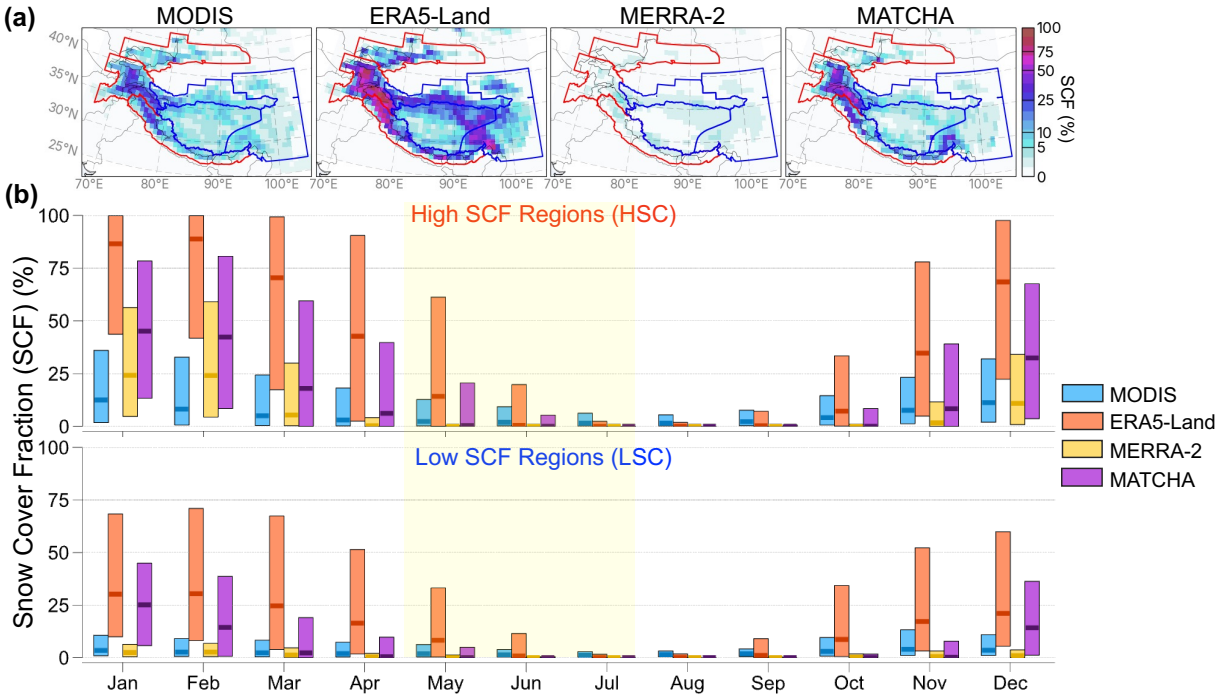


**Fig. S1. Spatio-temporal distribution of snow cover fraction over HMA**. (a) Temporal average (2003-2018) of snow cover fraction at 0.75° resolution during the late snowmelt season (May - July) with geographical outlines from RGI v6. Blue regions denote low snow cover (LSC) regions, while red regions denote high snow cover (HSC) regions. The LSC regions are composed of the following second-order regions based on the Randolph Glacier Inventory v6.0, 1) Inner Tibet, 2) S and E Tibet, 3) Hengduan Shan, 4) Qilian Shan, 5) W and E Tien Shan, 6) W and E Kun Lun. The HSC regions are composed of the following second-order regions, 1) W, C, and E Himalayas, 2) Hindu Kush, 3) Karakoram, 4) Pamir, and 5) Hissar Alay. (b) Monthly time series of snow cover fraction (SCF) across low and high snow cover regions from three reanalysis datasets and MODIS. The height of the bars represents the interquartile range (IQR) with the median.

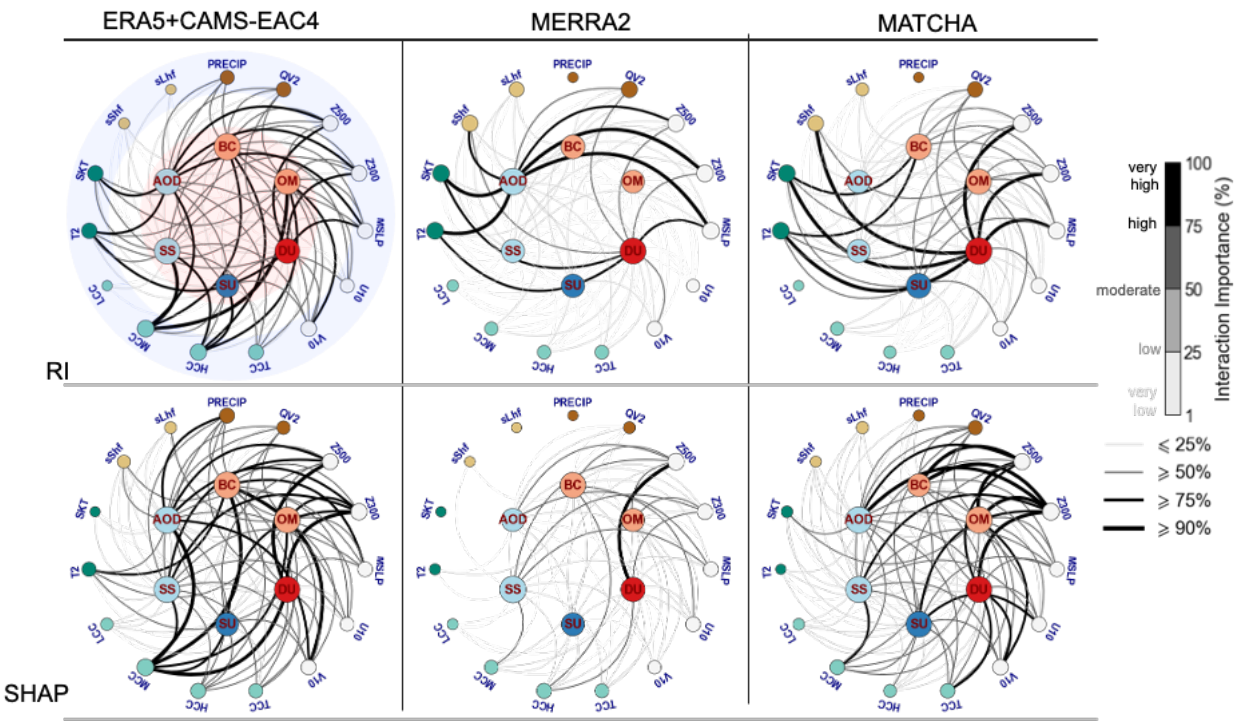


**Fig. S2. Underrepresented aerosol-meteorology interactions for all three reanalyses and each importance metric.** Network diagrams depicting the underrepresented interactions (positive difference in interaction importance from Obs-Model construct and Model-Model construct) for three reanalyses (across columns) and the importance metrics (across rows). The nodes are arranged in a concentric fashion, with the innermost nodes representing aerosol predictors (highlighted with light red shading) and the outermost nodes representing meteorology predictors (highlighted with light blue shading). The interaction importances are shown through edges connections/lines between the nodes and are weighted by colors and width denoting the strength of the importance (1 to 100%, very low-low for <=25%, low-moderate for 25% to 50%, moderate-high for 50% to 75%, and high-very high for >=75% shown in the color bars).

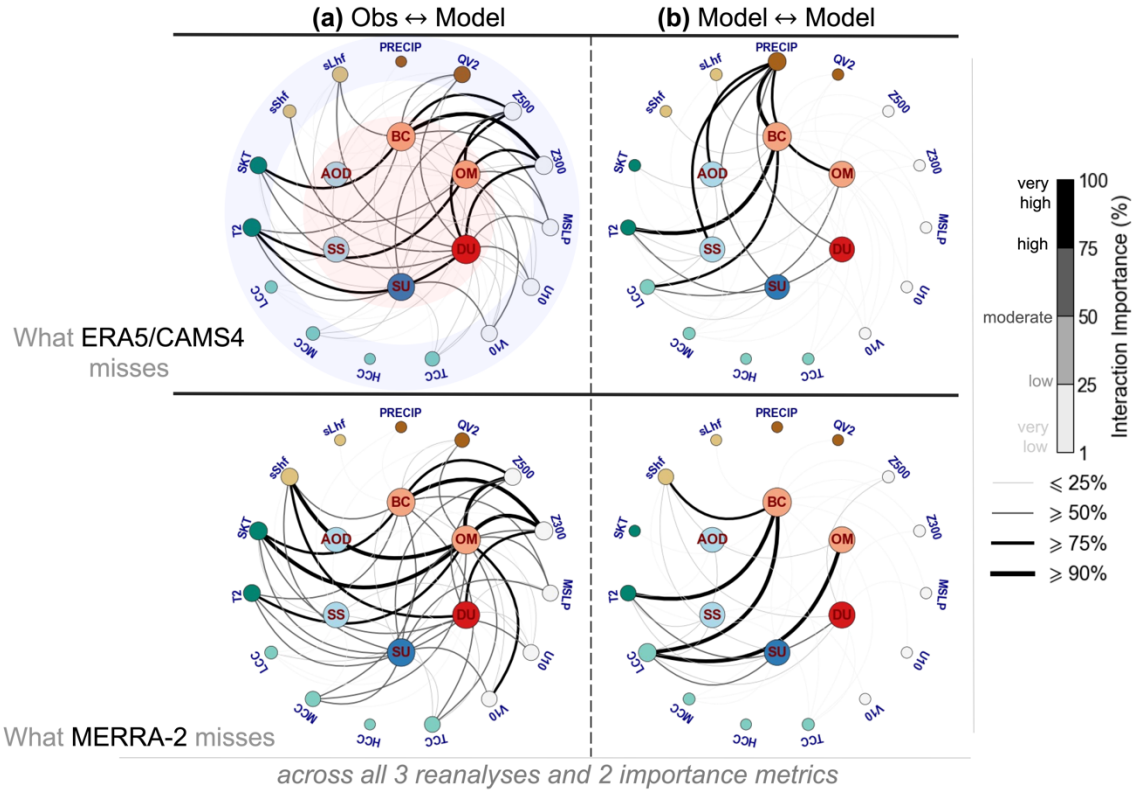


**Fig. S3. Underrepresented interactions that ERA5/CAMS4 and MERRA-2 fail to show relative to MATCHA.** Network diagrams depicting the underrepresented interactions in both reanalyses compared to MATCHA aggregated across both RI and SHAPc metrics for (a) Obs-Model and (b) Model-Model construct. The interaction importances are based on aerosol-meteorology interactions onto snow (AMI) in low snow-cover regions during the late snowmelt period (May-July). The nodes are arranged in a concentric fashion, with the innermost nodes representing aerosol predictors (highlighted with light red shading) and the outermost nodes representing meteorology predictors (highlighted with light blue shading). The interaction importances is shown through edges connections/lines between the nodes and are weighted by colors and width denoting the strength of the importance (1 to 100%, very low-low for <=25%, low-moderate for 25% to 50%, moderate-high for 50% to 75%, and high-very high for >=75% shown in the color bars).

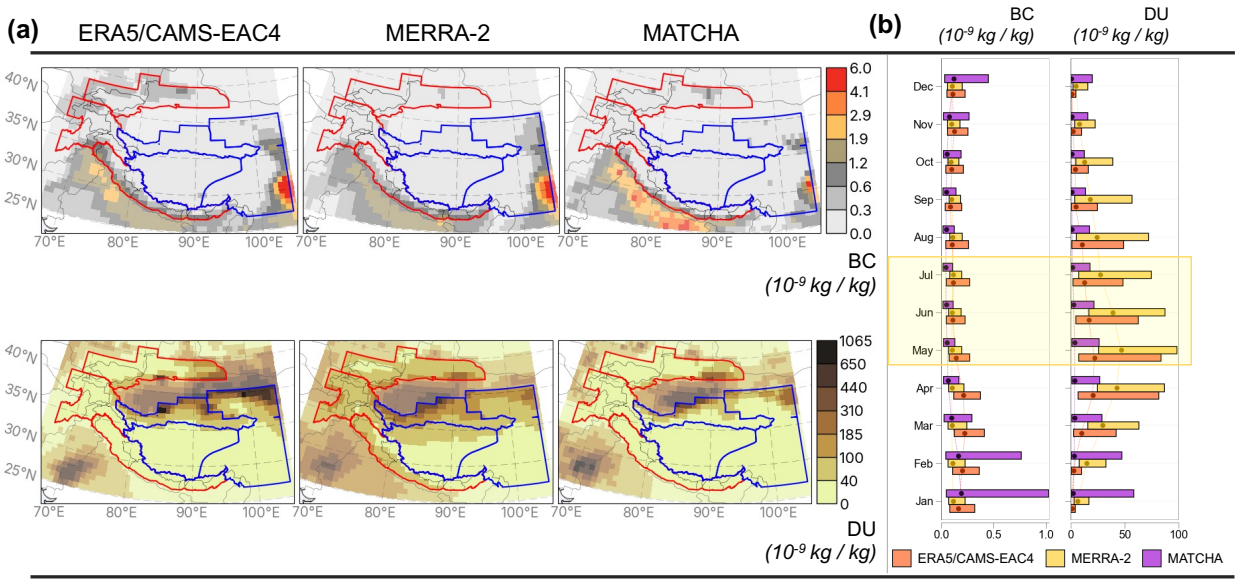


**Fig. S4.** Spatio-temporal distribution of surface black carbon (BC) and dust mixing ratios (DU) over HMA. (a) Temporal average (2003-2018) of BC and DU at a horizontal resolution of 0.75° used in our methodology across three reanalysis datasets during the late snowmelt season (May - July). Blue regions denote low snow cover (LSC) regions, while red regions denote high snow cover (HSC) regions. (b) Monthly time series of BC and DU across LSC regions for the three reanalysis datasets. The width of the bars represents the interquartile range (IQR) with the median denoted by dark circles. The shaded yellow region represents the time period (May-July) of our study.

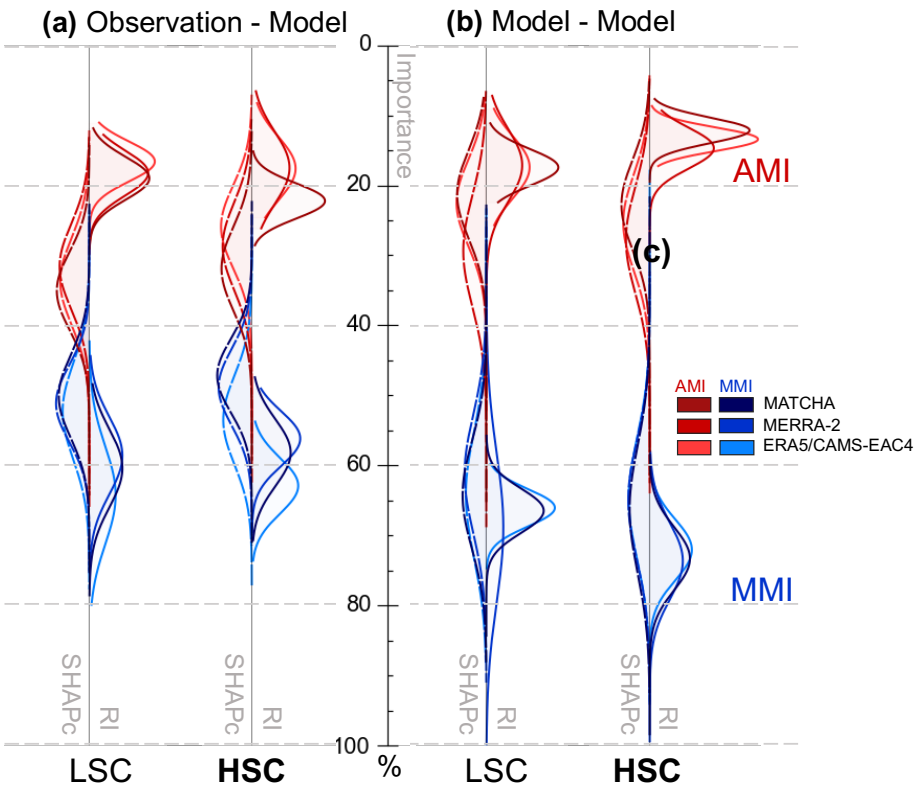


**Fig. S5. Importance of aerosol-meteorology interactions on snow in low and high snow-covered regions.** Distributions of importance metrics, relative importance (RI, solid), and Shapely contribution (SHAPc, dashed) for aerosol-meteorology (AMI) and meteorology-meteorology (MMI) interactions on snow shown for the Obs-Model (a) and Model-Model (c) construct across three reanalyses (ERA5/CAMS-EAC4, MERRA-2 and MATCHA).

**Table S3.** Overview of reanalysis and observation datasets used.

| | ERA5/CAMS-EAC4 | MERRA-2 | MATCHA |
|---|---|---|---|
| **Spatial Resolution** | 0.1° (ERA5-Land)<br>0.25° (ERA5)<br>0.75° (CAMS-EAC4) | 0.5° by 0.625° | 12 km |
| **Temporal Resolution** | hourly | hourly | hourly to 3-hourly |
| **Atmospheric Model** | IFS Cy41r2 | GEOS 5.12.4 | WRF v3.9.1 |
| **Land Model** | HTESSEL [1] | Catchment LSM [2] | CLM v4.5 – SNICAR [3] |
| **Snow Model** | 1 Layer | 3 Layer | 5 Layers |
| **Aerosol Model** | CAMS-IFS [4] | GOCART [5] | MOSAIC [6] |
| **Coupling Schemes** | None till date [a] | Aerosol-Radiation [b] | Aerosol-Radiation-Snow [c] |
| **Assimilated Observations** | | | |
| Snow | in-situ (not for >1500 m elevation locations)<br>IMS (4 km) | | |
| AOD | AATSR (Envisat)<br>MODIS Terra/Aqua | MISR<br>AERONET<br>MODIS Terra/Aqua | MODIS Terra/Aqua |
| CO | MOPITT CO (Total Column) | | MOPITT CO (Profile and Total Column) |

[a]Aerosol reanalysis from CAMS is not coupled to ERA5 meteorology which instead uses a monthly climatology for aerosols. Recent developments suggest a step towards incorporating aerosol coupling in the ECMWF IFS model [7].

[b]Aerosol reanalysis is radiatively coupled into the GEOS-5 model.

[c]Aerosol products are radiatively coupled with meteorology in WRF, while CLM-SNICAR couples aerosol deposition to snow properties.

**Table S4.** Overview of the variables used in our study.

| **Reanalysis** | | | | | |
|---|---|---|---|---|---|
| **Predictors** | **Group** | **Variable Name (with units)** | **ERA5/ERA5-L/CAMS** | **MERRA2** | **MATCHA** |
| | Carbonaceous | BC mixing ratio at the surface (kg/kg) | aermr09 | BCPHOLIC | BC_SFC_TOT |
| | | | aermr10 | BCPHOBIC | |
| | Carbonaceous | OM mixing ratio at the surface (kg/kg) | aermr07 | OCPHILIC | OC_SFC_TOT |
| | | | aermr08 | OCPHOBIC | |
| | Dust | DU mixing ratio at the surface (kg/kg) | aermr0(4-6) | DU00(1-5) | DUST_SFC_TOT |
| | Sulphate | SU mixing ratio at the surface (kg/kg) | aermr11 | SO4 | SO4_SFC_TOT |
| | Others | SS mixing ratio at the surface (kg/kg) | aermr0(1-3) | SS00(1-5) | NA_SFC_TOT |
| | Others | Aerosol optical depth at 550nm* | taod550 | TOTEXTTAU | AOD_550 |
| | Moisture | Daily Accumulated Precipitation (mm) | tp (ERA5-Land) | PRECTOTLAND | RAINC |
| | | | | | RAINNC |
| | Moisture | Specific Humidity (kg/kg) | d2m [a] | QV2M | Q2 |
| | Circulation | Geopotential Height at 500 hPa (m) | z | H | PHP |
| | Circulation | Geopotential Height at 300 hPa (m) | z | H | PHP |
| | Circulation | Mean Sea Level Pressure (Pa) | msl | SLP | P |
| | | | | | PB |
| | Circulation | Zonal Wind at 10 m (m/s) | u10 | U10M | U10 |
| | Circulation | Meridional Wind at 10 m (m/s) | v10 | V10M | V10 |
| | Cloud Cover (CC) [b] | Total CC | tcc | CLDTOT | CFRACT |
| | Cloud Cover (CC) | High CC [c] | hcc | CLDHGH | CFRACT |
| | Cloud Cover (CC) | Medium CC [d] | mcc | CLDMID | CFRACT |
| | Cloud Cover (CC) | Low CC [e] | lcc | CLDLOW | CFRACT |

| | | | | | |
|---|---|---|---|---|---|
| | Temperature | Temperature at 2 m (K) | t2m | T2M | T2 |
| | Temperature | Skin Temperature (K) | skt | TS | TSK |
| | Radiation | Surface Sensible Heat Flux (W/m2) | sshf | SHLAND | HFX |
| | Radiation | Surface Latent Heat Flux (W/m2) | slhf | LHLAND | LH |
| | Elevation | Elevation (m) | GMTED2010 | | |
| **Target** | | Snow Cover Fraction (%) | sc (ERA5-Land) | FRSNO | SNOWFRAC |
| **Observations** | | Snow Cover Fraction (%) | MOD10C1 | | |
| | | | MYD10C1 | | |
| | | Land Surface Temperature (K) | MOD11C1 | | |
| | | | MYD11C1 | | |
| | | AOD at 550 nm* | MCD19A2 | | |
| | | Daily Accumulated Precipitation (mm) | IMERG Final Run | | |

[a]Dewpoint at 2 m from ERA5 converted to specific humidity following Bolton, 1980[8].

[b]All cloud cover variables are in fraction (0-1).

[c]High cloud cover defined for model pressure levels < 0.4-0.45 $P_s$ hPa across all three reanalyses where $P_s$ is the surface pressure in hPa.

[d]Medium cloud cover defined with (0.4-0.8) $P_s$ hPa for ERA5 and MATCHA, while 400-700 hPa based on MERRA-2's model terrain following coordinate.

[e]Low cloud cover defined within (1 – 0.8) $P_s$ hPa for ERA5 and MATCHA while 1000-700 hPa based on MERRA-2's model terrain following coordinate.

*Aerosol optical depth at 550 nm is unitless.

## Supplementary References


1. Dutra, E., Balsamo, G., Viterbo, P., Miranda, P. M. A., Beljaars, A., Schär, C., and Elder, K.: An improved snow scheme for the ECMWF land surface model: Description and offline validation, J. Hydrometeorol., 11, 899–916, https://doi.org/10.1175/2010JHM1249.1, 2010.
2. Koster, R. D., Suarez, M. J., Ducharne, A., Stieglitz, M., and Kumar, P.: A catchment-based approach to modeling land surface processes in a general circulation model: 1. Model structure, J. Geophys. Res. Atmos., 105, 24809–24822, https://doi.org/10.1029/2000JD900327, 2000.
3. Flanner, M. G., Zender, C. S., Randerson, J. T., and Rasch, P. J.: Present-day climate forcing and response from black carbon in snow, J. Geophys. Res. Atmos., 112, D11202, https://doi.org/10.1029/2006JD008003, 2007.
4. Morcrette, J.-J., Boucher, O., Jones, L., Salmond, D., Bechtold, P., Beljaars, A., Benedetti, A., Bonet, A., Kaiser, J. W., Razinger, M., Schulz, M., Serrar, S., Simmons, A. J., Sofiev, M., Suttie, M., Tompkins, A. M., and Untch, A.: Aerosol analysis and forecast in the European Centre for Medium-Range Weather Forecasts Integrated Forecast System: Forward modelling, J. Geophys. Res. Atmos., 114, D06206, https://doi.org/10.1029/2008JD011235, 2009.
5. Chin, M., Ginoux, P., Kinne, S., Torres, O., Holben, B. N., Duncan, B. N., Martin, R. V., Logan, J. A., Higurashi, A., and Nakajima, T.: Tropospheric aerosol optical thickness from the GOCART model and comparisons with satellite and sun photometer measurements, J. Atmos. Sci., 59, 461–483, https://doi.org/10.1175/1520-0469(2002)059<0461:TAOTFT>2.0.CO;2, 2002.
6. Zaveri, R. A., Easter, R. C., Fast, J. D., and Peters, L. K.: Model for simulating aerosol interactions and chemistry (MOSAIC), J. Geophys. Res. Atmos., 113, D13204, https://doi.org/10.1029/2007JD008782, 2008.
7. Benedetti, A., and Vitart, F.: Can the direct effect of aerosols improve subseasonal predictability?, Mon. Weather Rev., 146, 3481–3498, https://doi.org/10.1175/MWR-D-17-0282.1, 2018.
8. Bolton, D.: The computation of equivalent potential temperature, Mon. Weather Rev., 108, 1046–1053, https://doi.org/10.1175/1520-0493(1980)108<1046:TCOEPT>2.0.CO;2, 1980.